Homeocurvature adaptation of phospholipids to high pressure in deep-sea invertebrates

Authors: Jacob R. Winnikoff[1,2,3,4*], Daniel Milshteyn[1], Sasiri J. Vargas-Urbano[5], Miguel A. Pedraza[5], Aaron M. Armando[6], Oswald Quehenberger[6], Alexander Sodt[7], Richard E. Gillilan[8], Edward A. Dennis[1,6], Edward Lyman[5], Steven H. D. Haddock[3,4], and Itay Budin[1*]

Affiliations:

[1]Department of Chemistry and Biochemistry, University of California San Diego; 9500 Gilman Dr., La Jolla, CA 92093, USA.

[2]Department of Organismic and Evolutionary Biology, Harvard University; 16 Divinity Ave., Cambridge, MA 02138, USA.

[3]Monterey Bay Aquarium Research Institute; 7700 Sandholdt Rd., Moss Landing, CA 95039, USA.

[4]Department of Ecology and Evolutionary Biology, University of California Santa Cruz; 1156 High St., Santa Cruz, CA 95064, USA.

[5]Department of Physics and Astronomy, University of Delaware; 210 South College Ave., Newark, DE 19716, USA.

[6]Department of Pharmacology, University of California San Diego Health Sciences; 9500 Gilman Dr., La Jolla, CA 92093, USA.

[7]Unit on Membrane Chemical Physics, National Institute of Child Health and Human Development; 29 Lincoln Drive, Bethesda, MD 20892

[8]Center for High-Energy X-ray Sciences, Ithaca, NY 14850

*Corresponding authors. Email: ibudin@ucsd.edu, jwinnikoff@g.harvard.edu

Abstract: Pressure increases with depth in the ocean, but little is known about the molecular bases of biological pressure tolerance. We describe a mode of pressure-adaptation in comb jellies (ctenophores) that also constrains these animals' depth range. Structural analysis of deep-sea ctenophore lipids showed that they form a non-bilayer phase, even under pressures at which it is usually not stable. Lipidomics and all-atom simulations identified non-bilayer phospholipids with strong negative spontaneous curvature as a hallmark of deep-adapted membranes that causes this phase behavior. Synthesis of higher-curvature lipids enhanced pressure tolerance in *Escherichia coli*, whereas low-curvature lipids had the opposite effect. Imaging indicates that the disintegration of deep-sea animals when brought to the surface could be driven by the phase behavior of their phospholipids.

One-Sentence Summary: High-curvature phospholipids are a hallmark of deep-sea ctenophore membranes and support biological function at extreme pressures.

Main Text

The deep sea encompasses more than 90% of Earth's habitable volume and is characterized by low temperature and high pressure, with the pressure increasing by about 1 bar per 10 m depth. In contrast to low-temperature adaptation, few specific mechanisms of pressure

tolerance in animals are known (*1*). Pressure inhibits high-volume conformations of all biomolecules, but has an especially strong effect on lipids because of the high compressibility of their hydrocarbon chains (*2*). Phospholipid membranes generally exist in a liquid-crystalline state known as the fluid lamellar (L_α) phase. When an L_α membrane are subjected to pressure, their packing increases, reducing fluidity and, eventually, causing a transition to a gel (L_β) phase like that induced by cold (*3*). For this reason, it has been largely assumed that the phospholipids of marine ectotherms adapt similarly to low temperature and high pressure by increasing acyl chain unsaturation and decreasing chain length to counteract the reduction of membrane fluidity by both conditions (*2–4*). However, phospholipid compressibility is also highly anisotropic, meaning that pressure has a strong effect on overall lipid shape. Lipids like phosphatidylethanolamine (PE) have a conical steric profile, which is rendered more cylindrical by high pressure. Conical lipids are important for membrane protein function (*5*) and favor the formation of non-lamellar intermediates for fusion and fission, such as the inverse hexagonal (H_{II}) phase (*6*).

We investigated high-pressure adaptation in comb jellies (phylum Ctenophora): soft-bodied, poikilothermic invertebrates that inhabit diverse ocean environments. In situ observations (Fig. 1B), showed that multiple ctenophore lineages adapted independently to various depths (*7*), making ctenophores a useful comparative system for studying deep-sea adaptation. In addition to their depth distributions, ctenophores show physiological responses consistent with pressure-specialization. When exposed to high pressures, shallow-adapted ctenophores exhibit constant, accelerated beating of their comb rows (Movie S1) leading to eventual shearing (Fig. S1A, S1B). Loss of motor control in ctenophores and other animals (*8*) could implicate failure at synapses (*9*), which are enriched in cone-shaped lipids (*10*). In contrast, when deep-constrained species are brought isothermally to atmospheric pressure, their tissues disintegrate (Fig. 1A, Fig. S1C), a phenomenon also documented across several phyla (*11*, *12*). When imaged by spectral confocal microscopy, ectodermal tissue dissected from deep-constrained ctenophores showed a loss of membrane structure and an abrupt increase in the General Polarization (GP) of the fluorescent membrane label C-Laurdan – a lipid packing sensor – during disintegration (Fig. 1C). We did not observe this phenomenon in a shallow-constrained ctenophore species, whose habitat extends to the surface, that we collected on the same Remotely Operated Vehicle dive. We tested whether pressure effects on cell membranes could underlie ctenophores' physiological tolerances and depth ranges.

Deep-sea membrane lipids exist in non-lamellar phases, even under high pressure

We probed structural signatures of pressure adaptation in deep-sea membranes by High-Pressure Small Angle X-Ray Scattering (HPSAXS) (*13*) and High-Pressure Fluorescence Spectroscopy (HPFS). In HPSAXS, phospholipids produce X-ray scattering patterns (Fig. 2B) from which major phase changes, i.e. changes in the mobility and arrangement of lipids, can be identified. We used reconstituted polar lipid extracts, to map the predominance of the lamellar fluid (L_α), lamellar gel (L_β), and non-lamellar inverted hexagonal (H_{II}) phases across pressure-temperature (P-T) space (Fig. 2C). Within lamellar regimes, membrane fluidity was assessed by HPFS measuring C-Laurdan General Polarization (GP) (Figs. 2D, S1F). We used these approaches to analyze lipid extracts from 5 species (8 animals total) that provided sufficient biomass and were native to different domains of depth (0 - 4000 m, collected by SCUBA and ROV) and temperature (0 - 20°C, collected at different latitudes) (Fig. 2A). The comparison of *Beroe cucumis* from Arctic surface waters with Platyctenida sp. T. from the seafloor at ~4000 m was particularly informative, due to the similar temperatures but drastically different pressures of

their environments. Although these analyses did not sample any single membrane in the organism nor account for membrane proteins or osmolytes, they allowed us to compare phase behavior trends intrinsic to lipids.

All ctenophore lipid extracts formed an L_α phase in the native P-T domain of the source animal. Within this phase, membrane fluidity was higher in both deep and shallow-cold samples than in temperate samples, consistent with homeoviscous adaptation (Fig. 2D). Pressure-dependent gel phase transitions ($L_\alpha \rightarrow L_\beta$) were observed at moderate pressures (~200 bar) in lipids from shallow temperate animals and at much higher pressures (>1000 bar) in species from deep water. However, Arctic species inhabiting shallow water, which are adapted to cold but not to high pressure, showed a gel phase transition indistinguishable from that of species that dwell in the deep sea. In contrast, there was a consistent relationship between the animals' native P-T and the non-lamellar phase transition ($L_\alpha \rightarrow H_{II}$) of their lipids. In the species from the deepest environment sampled, decreasing pressure ~200 bar from the native P-T – analogous to moving 2000 m shallower in an isothermal seawater column – caused lipids to invert to H_{II}, which coincided with non-monotonic trends in C-Laurdan GP. Similar habitat-specific patterns were observed in samples from a pair of closely related depth-specialist species that adapted independently to surface and deep waters (Fig. S1D, E, F). Thus, the deep-sea lipids we analyzed did not show reduced sensitivity to the $L_\alpha \rightarrow L_\beta$ transition (*14*) compared to those from shallow, cold-water animals, but did show enhanced access to the $L_\alpha \rightarrow H_{II}$ transition, which is modulated by lipid shape.

Ctenophore lipids show contrasting adaptations to pressure and cold

To identify the lipids responsible for pressure-specific physical properties, we analyzed ctenophores collected across a 4000-m depth range, as well as from surface waters at tropical, temperate, and polar latitudes (Fig. 3A, Table S1). This global sampling enabled us to distinguish adaptations to high pressure from those to cold, as temperature also decreases in deeper ocean waters. Phospholipids were the dominant type of polar lipids in all 66 ctenophores sampled (across 17 species) but their headgroup composition displayed divergent relations to high pressure and low temperature (Fig. 3B). Depth was associated with a 5-fold increase in the abundance of plasmenyl phosphatidylethanolamine (PPE), which contains an *sn*-1 α-alkenyl ether linkage (*15*). Based on a phylogeny inferred from transcriptomes, depth-associated PPE accumulation appears to have evolved independently at least three times in ctenophores (Fig. 3C). PPE was not associated with cold-adaptation independent of depth; in fact, it was more abundant in warm-water shallow-adapted animals than cold-water ones. Animals from shallow, cold water had high amounts of phosphatidylcholine (PC), a cylindrical lipid that increases membrane fluidity and is observed in cold-adapted poikilotherms (*16*). Outside of phospholipids, ctenophore lipidomes contained small amounts of cholesterol (<5%), with the notable exception of warm-water animals, and low amounts of sphingomyelin (<0.5%) (Fig. S2C).

In addition to headgroups, divergent trends were seen in phospholipid acyl chains. Acyl chain unsaturation followed trends consistent with homeoviscous adaptation: the number of double bonds increased with both increasing depth and decreasing temperature. However, acyl chain length increased in samples from deeper habitats, in contrast to those from cold, shallow water and to the pattern predicted by homeoviscosity (Fig. 3D). P-T trends were most apparent when all acyl chains were averaged, however the *sn*-1 chains alone exhibited strong signals. The patterns among *sn*-2 chains were similar but not statistically significant (Fig. S2A). Acyl chain analysis of lysophosphatidylethanolamine (LPE) also indicated that variation in PPE abundance between samples was not driven by oxidative degradation (Fig. S2B). These results indicate that

ctenophore lipidomes contain depth-specific adaptations that cannot be fully explained by a need to maintain membrane fluidity. Although our analysis could not resolve ctenophore membrane composition at a subcellular level, the homogeneity of deep and cold-water lipidomes, containing predominantly polyunsaturated PC or PPE, suggest that they do not feature the extensive heterogeneity characteristic of mammalian cell membranes (*17*).

Biophysical measurements and simulations support a homeocurvature adaptation model

We analyzed the pressure-dependent properties of PPE, given that it was the only major depth-correlated lipid class (Fig. S2C) and constituted up to 73% of phospholipids in whole bodies – and slightly more in tentacle tissue – from the samples obtained at greatest depth (Fig. S2D). The midpoint pressure for the inverted phase transition ($L_\alpha \rightarrow H_{II}$) was higher for liposomes composed of PPE, with either monounsaturated or polyunsaturated *sn*-2 chains, than those made of the corresponding PE species. The pressure of the gel phase transition ($L_\alpha \rightarrow L_\beta$) also slightly increased, both shifting and narrowing the fluid lamellar region (Fig. 4A, Fig. S3A). Within the lamellar phase, PPE increased membrane fluidity at high pressures (Fig. S3B). High membrane fluidity and the ability of lipids to form non-lamellar topologies like H_{II} are thought to be required for membrane fusion (*17*). Accordingly, we found that Ca^{2+}-mediated fusion of liposomes *in vitro* was inhibited by moderate pressures (100 bar), but that this loss of activity could be restored by substitution of PPE for PE (Fig. S4).

In light of the distinctive phase behavior of PPE, we tested whether there is a broader depth-adaptive trend in lipid shape. The conical or cylindrical nature of a lipid's steric profile is captured in the monolayer spontaneous curvature parameter c_0. This curvature, which has units of inverse length, is defined as the reciprocal of the radius circumscribed by an unstressed monolayer of a given lipid. A negative-curvature lipid forms monolayers curving toward the headgroup, as are observed in the H_{II} phase, whereas a zero-curvature lipid forms flat monolayers, thus favoring lamellar phases. It has remained unclear whether the propensity for PPE to promote the H_{II} phase corresponds to a more negative c_0 (also termed "higher curvature") for the lipid class (*18*, *19*). We measured the pressure-dependent c_0 of PPE relative to that of diacyl PE using HPSAXS and found that it was more negatively curved under all conditions, requiring 700 bar of pressure to match the curvature of PE (Fig. 4B). PPE thus has the most negative curvature of any phospholipid class, although we cannot rule out other mechanisms by which it could promote the H_{II} phase. Based on these curvature values and previous measurements, we built a model that calculates the mean lipidome curvature at 1 bar, $\bar{c_0}$, incorporating contributions from headgroup classes (Fig. 4C), lysolipids, and *sn*-1 acyl chain structure (Materials and Methods). Modeled $\bar{c_0}$ becomes more negative with habitat depth among cold-adapted ctenophores (Fig. S5C), as well as among all individuals (Fig. 4D). It does not correlate with temperature (Figs. 4D, S5D). The model also predicts that in shallow-warm animals, PPE negative curvature is offset by positively curved lysolipids and lower chain unsaturation (Fig. S5A).

The formula for $\bar{c_0}$ assumes ideal mixing of lipids, which is not the case in complex mixtures that typically compose cell membranes. To address this, we conducted molecular dynamics (MD) simulations of bilayers modeled after ctenophore lipidomes. Simulations were performed with all-atom resolution using the Chemistry at HARvard Macromolecular Mechanics v36 (CHARMM36) force-field, which we were able to validate at high pressure (Supplementary Text) by predicting experimentally observed pressure-dependent changes to bilayer packing parameters and phase transitions (Fig. S6). We constructed complex membranes containing representatives of the predominant (≥5%) lipid classes, including both phospholipids and

cholesterol (Fig. S7A). When comparing cold-adapted Platyctenida sp. T (4000 m, 2°C) with *Bolinopsis infundibulum* (10 m, 0°C), whose lipidome is similar to that of *Beroe cucumis* used in HPSAXS (Fig. S2E), we observed similar pressure-dependencies for lipid packing (APL strain) and translational mobility (D_T). However, the first moment of the lateral stress profiles – a measure of membrane deformability that is equal to the negative product of the monolayer bending modulus (k_b) and spontaneous curvature (c_0) – displayed a large (~500 bar) pressure offset (Fig. 4E). Although simulations were constrained to a bilayer state, the high $-k_b c_0$ values of Platyctenida sp. T lipids at low pressures was consistent with their tendency to form the non-lamellar H_{II} phase, as observed by HPSAXS.

We simulated two additional species from different P-T regimes: *Lampocteis cruentiventer* (630 m, 5°C) and *Bolinopsis vitrea* (10 m, 26°C) (Fig. S7). The *L. cruentiventer* simulations produced APL strain and D_T values indistinguishable from those of the other two cold species and a smaller $-k_b c_0$ than that of *B. infundibulum*. Because all simulations were done at 20°C and *L. cruentiventer* lives in a habitat warmer than those of *B. infundibulum* and Platyctenida sp. T, this difference could reflect the interplay between temperature- and depth-adaptation. In simulation, *B. vitrea* lipids exhibited the lowest values for $-k_b c_0$ across simulated pressures (Fig. S7B), further indicating that lipidome components, including acyl chain composition, positively curved lipids, and cholesterol content, counterbalance the negative curvature of PPE in animals adapted to warm, shallow conditions. At 1000 bar, *B. vitrea* bilayers exhibited regions of condensed, gel-like chains (Fig. S7D) that were not observed in the three cold-water species, consistent with the behavior of samples from the warmest shallow conditions analyzed by HPSAXS (Fig. 2C).

Based on these analyses, we propose a *homeocurvature adaptation model* for depth specialization (Fig. 4F). In this model, phospholipids with more negative curvature (as measured at 1 bar) are required to maintain transmembrane protein function and membrane plasticity at higher pressure. In animals from deep, high-pressure environments, this requirement results in lipid compositions that do not form stable bilayers when depressurized. Consistent with this tradeoff, the increasing C-Laurdan GP of disintegrating *Bathocyroe* ($\overline{c_0}$ = -0.013 +/- 1.9×10^{-3} Å^{-1}) cell membranes in Fig. 1 resembled that of synthetic (Fig. S3B) and animal-derived (Fig. 2D, Fig. S1F) liposomes inverting to form H_{II}. In contrast, the shallow-constrained species *Bolinopsis microptera* ($\overline{c_0}$ = -0.0058 +/- 6.0×10^{-4} Å^{-1}), which does not disintegrate, showed a decrease in GP under the same conditions, consistent with its membranes remaining lamellar and becoming more fluid as they were warmed (Fig. 1C, S8A).

Modulating lipid curvature can enhance or reduce biological pressure tolerance

We sought to test the key prediction of the homeocurvature adaptation model – that lipidome curvature modulates biological pressure tolerance – using laboratory organisms whose membrane composition could be genetically manipulated. The inner membrane of *E. coli* strain K12 is composed primarily of PE, with acyl chains that maintain both fluidity (*20*) and curvature (*4*) in response to temperature changes. To test the effects of more negative lipidome curvature, we expressed a PPE synthesis cassette (plsAR) from *Clostridium perfringens (21)* in anaerobically grown *Escherichia coli* strain BL21 (Fig. 5A), then exposed the cultures to high pressure for 48 hours. Upon induction of plsAR expression, 25% of total phospholipids were converted from PE to PPE (Fig. S9A), while the acyl chain profile remained similar (Fig. S9B). SAXS analysis of reconstituted *E. coli* lipid extracts showed that plsAR expression promoted the H_{II} phase relative to the empty-vector control, consistent with an increase in negative phospholipid curvature (Fig. 5B, S9C). When BL21 with and without plsAR was grown at 500

bar, both the doubling rate and survival of PPE-synthesizing cells were significantly less pressure-sensitive than those of the empty-vector control (Fig. 5C and D).

To test the effects of reduced negative lipidome curvature on high-pressure fitness, we used a P_{BAD}-PC synthase cassette (*22*) to replace PE with PC. PC has a higher fluidity than PE and better resists pressure-induced gelling (Fig. S3D), but its cylindrical profile inhibits non-lamellar topologies (*23*). It can thus be used to differentiate the effects of membrane fluidity and gel phase transitions from those related to curvature. SAXS analysis confirmed that lipids from PC-synthesizing cells formed a less stable H_{II} phase and were also more resistant to the gel phase transition (Figs. 5F, S9C). Growth of PC-producing cells was diminished at 250 bar and survival ceased at 500 bar (Fig. 5G, H), indicating that loss of lipid curvature is deleterious to high-pressure fitness even when fluidity is increased. Both PC- and PPE-synthesizing strains also showed lower levels of phosphatidylglycerol (PG), but loss of PG synthesis alone did not alter high-pressure fitness under our experimental conditions (Fig. S9D, E). Therefore, increase (by PPE synthesis) or decrease (by PC synthesis) of negative lipidome curvature can be sufficient to modulate high-pressure fitness in cells.

Discussion

All biological membranes consist of cylindrical bilayer-forming lipids, which support membrane structure, and conical non-bilayer lipids, which support membrane plasticity (*25*). The high-pressure and low-temperature waters of the deep sea present a biophysical challenge to maintaining the latter. Reconstituted deep-sea lipids can adopt non-lamellar topologies like the H_{II} phase, even under these extreme conditions. Multiple molecular adaptations underlie this capability. The ether phospholipid PPE, a major component of deep-sea ctenophore membranes, maintains a conical shape under high-pressure deep-sea conditions because of its highly negative spontaneous curvature. We also observed increased abundance of PPE in tropical surface animals, where it could fulfill roles as an antioxidant (*26*) and as a driver of local heterogeneity in cholesterol-rich membranes (*27*). Exclusive to samples from deep waters was the combination of abundant PPE, long and highly unsaturated acyl chains, and low amounts of lysolipids, all of which contribute to lipidomes with exceptionally negative spontaneous curvature at 1 bar. High pressure reduces this extreme curvature so that deep lipidomes form physiologically viable membranes under their native conditions.

Lipid adaptation in marine systems has mostly been explored in the context of temperature, with pressure- and cold-adaptation treated as functionally interchangeable. However, pressure is a stronger inhibitor of non-lamellar topologies because of their large molar volume. In contrast, temperature is dominant in controlling membrane fluidity and the formation of gel phases. Accordingly, we found that depth-adaptation in ctenophores is biochemically distinct from cold-adaptation. The hallmark of shallow, low-temperature lipidomes is a high fraction of low-melting-temperature PC lipids with shorter acyl chains, whose abundance decreases with depth. In contrast, deep-sea animals accumulate conical non-bilayer lipids, including PPE, which has both stronger curvature and greater fluidity than diacyl PE. These differing responses to cold and pressure suggest that deeper environments might not substitute for contracting regions with cold surface waters, which has been proposed as a mechanism of ecological resilience in warming polar seas (*28*).

The homeocurvature adaptation model postulates that pressure-induced changes in lipid shape are relevant to the habitat ranges of both shallow and deep animals (Fig. 4F). The loss of motor function in shallow-constrained animals subjected to high pressure (Movie S1, Fig. S1A, B) is consistent with membrane-associated defects in the nervous system, for example in

synaptic vesicle trafficking or ion channel function. Animals specialized to deep habitats may mitigate such defects by accumulating high-curvature lipids, which are also enriched in the nervous systems of mesophiles (*29*). Because it is based on hydrocarbon compressibility, the effect of pressure on lipid shape is similar in all phospholipids, so counteracting it requires a more negative baseline (1 bar) curvature that may not sustain a lamellar phase at the surface. Through this mechanism, adaptation to extreme depths could have given rise to organisms that require pressure to maintain their membranes.

References

1. P. H. Yancey, M. E. Gerringer, J. C. Drazen, A. A. Rowden, A. Jamieson, Marine fish may be biochemically constrained from inhabiting the deepest ocean depths. *Proc. Natl. Acad. Sci.* **111**, 4461–4465 (2014).
2. G. N. Somero, Adaptations to High Hydrostatic Pressure. *Annu. Rev. Physiol.* **54**, 557–577 (1992).
3. A. R. Cossins, A. G. Macdonald, The adaptation of biological membranes to temperature and pressure: Fish from the deep and cold. *J. Bioenerg. Biomembr.* **21**, 115–135 (1989).
4. S. Morein, A.-S. Andersson, L. Rilfors, G. Lindblom, Wild-type *Escherichia coli* Cells Regulate the Membrane Lipid Composition in a "Window" between Gel and Non-lamellar Structures. *J. Biol. Chem.* **271**, 6801–6809 (1996).
5. M. Wikström, A. A. Kelly, A. Georgiev, H. M. Eriksson, M. R. Klement, M. Bogdanov, W. Dowhan, Å. Wieslander, Lipid-engineered Escherichia coli Membranes Reveal Critical Lipid Headgroup Size for Protein Function. *J. Biol. Chem.* **284**, 954–965 (2009).
6. P. I. Kuzmin, J. Zimmerberg, Y. A. Chizmadzhev, F. S. Cohen, A quantitative model for membrane fusion based on low-energy intermediates. *Proc. Natl. Acad. Sci.* **98**, 7235–7240 (2001).
7. J. R. Winnikoff, S. H. D. Haddock, I. Budin, Depth- and temperature-specific fatty acid adaptations in ctenophores from extreme habitats. *J. Exp. Biol.* **224**, jeb242800 (2021).
8. G. L. Kooyman, *Diverse Divers* (Springer Berlin Heidelberg, Berlin, Heidelberg, 1989), vol. 23 of *Zoophysiology*.
9. P. Burkhardt, J. Colgren, A. Medhus, L. Digel, B. Naumann, J. J. Soto-Angel, E.-L. Nordmann, M. Y. Sachkova, M. Kittelmann, Syncytial nerve net in a ctenophore adds insights on the evolution of nervous systems. *Science*. **380**, 293–297 (2023).
10. S. Takamori, M. Holt, K. Stenius, E. A. Lemke, M. Grønborg, D. Riedel, H. Urlaub, S. Schenck, B. Brügger, P. Ringler, S. A. Müller, B. Rammner, F. Gräter, J. S. Hub, B. L. De Groot, G. Mieskes, Y. Moriyama, J. Klingauf, H. Grubmüller, J. Heuser, F. Wieland, R. Jahn, Molecular Anatomy of a Trafficking Organelle. *Cell.* **127**, 831–846 (2006).
11. M. E. Gerringer, J. C. Drazen, T. D. Linley, A. P. Summers, A. J. Jamieson, P. H. Yancey, Distribution, composition and functions of gelatinous tissues in deep-sea fishes. *Royal Society Open Science*. **4**, 171063 (2017).
12. J. J. Childress, A. T. Barnes, L. B. Quetin, B. H. Robison, Thermally protecting cod ends for the recovery of living deep-sea animals. *Deep Sea Res. Part I*. **25**, 419–422 (1978).
13. D. K. Rai, R. E. Gillilan, Q. Huang, R. Miller, E. Ting, A. Lazarev, M. W. Tate, S. M. Gruner, High-pressure small-angle X-ray scattering cell for biological solutions and soft materials. *J. Appl. Crystallogr.* **54**, 111–122 (2021).
14. A. Maiti, S. Daschakraborty, Can Urea and Trimethylamine- *N* -oxide Prevent the Pressure-Induced Phase Transition of Lipid Membrane? *J. Phys. Chem. B.* **126**, 1426–1440 (2022).

15. J. M. Dean, I. J. Lodhi, Structural and functional roles of ether lipids. *Protein Cell*. **9**, 196–206 (2018).
16. R. Dawaliby, C. Trubbia, C. Delporte, C. Noyon, J.-M. Ruysschaert, P. Van Antwerpen, C. Govaerts, Phosphatidylethanolamine Is a Key Regulator of Membrane Fluidity in Eukaryotic Cells. *J. Biol. Chem.* **291**, 3658–3667 (2016).
17. J. H. Lorent, K. R. Levental, L. Ganesan, G. Rivera-Longsworth, E. Sezgin, M. Doktorova, E. Lyman, I. Levental, Plasma membranes are asymmetric in lipid unsaturation, packing and protein shape. *Nat. Chem. Biol.* **16**, 644–652 (2020).
18. K. Lohner, P. Balgavy, A. Hermetter, F. Paltauf, P. Laggner, Stabilization of non-bilayer structures by the etherlipid ethanolamine plasmalogen. *Biochimica et Biophysica Acta (BBA) – Biomembranes*. **1061**, 132–140 (1991).
19. K. Lohner, Is the high propensity of ethanolamine plasmalogens to form non-lamellar lipid structures manifested in the properties of biomembranes? *Chem. Phys. Lipids*. **81**, 167–184 (1996).
20. M. Sinensky, Homeoviscous Adaptation – A Homeostatic Process that Regulates the Viscosity of Membrane Lipids in *Escherichia coli*. *Proc. Natl. Acad. Sci.* **71**, 522–525 (1974).
21. D. R. Jackson, C. D. Cassilly, D. R. Plichta, H. Vlamakis, H. Liu, S. B. Melville, R. J. Xavier, J. Clardy, Plasmalogen Biosynthesis by Anaerobic Bacteria: Identification of a Two-Gene Operon Responsible for Plasmalogen Production in *Clostridium perfringens*. *ACS Chem. Biol.* **16**, 6–13 (2021).
22. M. Bogdanov, P. Heacock, Z. Guan, W. Dowhan, Plasticity of lipid-protein interactions in the function and topogenesis of the membrane protein lactose permease from *Escherichia coli*. *Proc. Natl. Acad. Sci.* **107**, 15057–15062 (2010).
23. R. Winter, A. Landwehr, T. Brauns, J. Erbes, C. Czeslik, O. Reis, "High-Pressure Effects on the Structure and Phase Behavior of Model Membrane Systems" in *High Pressure Effects in Molecular Biophysics and Enzymology*, J. L. Markley, D. B. Northrop, C. A. Royer, Eds. (Oxford University Press, 1996).
24. P. T. C. So, S. M. Gruner, S. Erramilli, Pressure-induced topological phase transitions in membranes. *Phys. Rev. Lett.* **70**, 3455–3458 (1993).
25. S. M. Gruner, Intrinsic curvature hypothesis for biomembrane lipid composition: a role for nonbilayer lipids. *Proc. Natl. Acad. Sci.* **82**, 3665–3669 (1985).
26. A. Broniec, R. Klosinski, A. Pawlak, M. Wrona-Krol, D. Thompson, T. Sarna, Interactions of plasmalogens and their diacyl analogs with singlet oxygen in selected model systems. *Free Radical Biology and Medicine*. **50**, 892–898 (2011).
27. L. J. Pike, X. Han, K.-N. Chung, R. W. Gross, Lipid Rafts Are Enriched in Arachidonic Acid and Plasmenylethanolamine and Their Composition Is Independent of Caveolin-1 Expression: A Quantitative Electrospray Ionization/Mass Spectrometric Analysis. *Biochemistry*. **41**, 2075–2088 (2002).
28. D. Cottin, A. Brown, A. Oliphant, N. C. Mestre, J. Ravaux, B. Shillito, S. Thatje, Sustained hydrostatic pressure tolerance of the shallow water shrimp *Palaemonetes varians* at different temperatures: Insights into the colonisation of the deep sea. *Comp. Biochem. Physiol. A Mol. Integr. Physiol.* **162**, 357–363 (2012).
29. X. Han, D. M. Holtzman, D. W. McKeel, Plasmalogen deficiency in early Alzheimer's disease subjects and in animal models: molecular characterization using electrospray ionization mass spectrometry: Plasmalogen Deficiency in Alzheimer's Disease. *J. Neurochem.* **77**, 1168–1180 (2001).

30. B. Schlining, N. Stout, *MBARI's Video Annotation and Reference System* (IEEE, 2006).

31. I. Budin, A. Debnath, J. W. Szostak, Concentration-Driven Growth of Model Protocell Membranes. *J. Am. Chem. Soc.* **134**, 20812–20819 (2012).
32. D. M. Owen, C. Rentero, A. Magenau, A. Abu-Siniyeh, K. Gaus, Quantitative imaging of membrane lipid order in cells and organisms. *Nat. Protoc.* **7**, 24–35 (2012).
33. E. G. Bligh, W. J. Dyer, A rapid method of total lipid extraction and purification. *Can. J. Biochem. Physiol.* **37**, 911–917 (1959).
34. G. Hamilton, K. Comai, Rapid separation of neutral lipids, free fatty acids and polar lipids using prepacked silica Sep-Pak columns. *Lipids.* **23**, 1146–1149 (1988).
35. H. Chung, M. Caffrey, The curvature elastic-energy function of the lipid–water cubic mesophase. *Nature.* **368**, 224–226 (1994).
36. Y.-F. Chen, K.-Y. Tsang, W.-F. Chang, Z.-A. Fan, Differential dependencies on [Ca^{2+}] and temperature of the monolayer spontaneous curvatures of DOPE, DOPA and cardiolipin: effects of modulating the strength of the inter-headgroup repulsion. *Soft Matter.* **11**, 4041–4053 (2015).
37. S. De Villiers, B. K. Nelson, Detection of Low-Temperature Hydrothermal Fluxes by Seawater Mg and Ca Anomalies. *Science.* **285**, 721–723 (1999).
38. B. Hopkins, R. E. Gillilan, S. Skou, *BioXTAS RAW*: improvements to a free open-source program for small-angle X-ray scattering data reduction and analysis. *J. Appl. Crystallogr.* **50**, 1545–1553 (2017).
39. O. Quehenberger, A. M. Armando, A. H. Brown, S. B. Milne, D. S. Myers, A. H. Merrill, S. Bandyopadhyay, K. N. Jones, S. Kelly, R. L. Shaner, C. M. Sullards, E. Wang, R. C. Murphy, R. M. Barkley, T. J. Leiker, C. R. H. Raetz, Z. Guan, G. M. Laird, D. A. Six, D. W. Russell, J. G. McDonald, S. Subramaniam, E. Fahy, E. A. Dennis, Lipidomics reveals a remarkable diversity of lipids in human plasma. *J. Lipid Res.* **51**, 3299–3305 (2010).
40. J. Hartler, A. M. Armando, M. Trötzmüller, E. A. Dennis, H. C. Köfeler, O. Quehenberger, Automated Annotation of Sphingolipids Including Accurate Identification of Hydroxylation Sites Using MS^n Data. *Anal. Chem.* **92**, 14054–14062 (2020).
41. N. Düzgünes, J. Wilschut, R. Fraley, D. Papahadjopoulos, Studies on the mechanism of membrane fusion. Role of head-group composition in calcium- and magnesium-induced fusion of mixed phospholipid vesicles. *Biochimica et Biophysica Acta (BBA) - Biomembranes.* **642**, 182–195 (1981).
42. T. Weber, B. V. Zemelman, J. A. McNew, B. Westermann, M. Gmachl, F. Parlati, T. H. Söllner, J. E. Rothman, SNAREpins: Minimal Machinery for Membrane Fusion. *Cell.* **92**, 759–772 (1998).
43. W. Tate, S. M. Gruner, Temperature dependence of the structural dimensions of the inverted hexagonal (HII) phase of phosphatidylethanolamine-containing membranes. *Biochemistry.* **28**, 4245–4253 (1989).
44. M. P. K. Frewein, M. Rumetshofer, G. Pabst, Global small-angle scattering data analysis of inverted hexagonal phases. *J. Appl. Crystallogr.* **52**, 403–414 (2019).
45. K. Dymond, Lipid monolayer spontaneous curvatures: A collection of published values. *Chem. Phys. Lipids.* **239**, 105117 (2021).
46. J. B. Klauda, R. M. Venable, J. A. Freites, J. W. O'Connor, D. J. Tobias, C. Mondragon-Ramirez, I. Vorobyov, A. D. MacKerell Jr, R. W. Pastor, Update of the CHARMM all-atom additive force field for lipids: validation on six lipid types. *J. Phys. Chem. B.* **114**, 7830–7843 (2010).

47. N. Leonard, R. W. Pastor, J. B. Klauda, Parameterization of the CHARMM All-Atom Force Field for Ether Lipids and Model Linear Ethers. *J. Phys. Chem. B.* **122**, 6744–6754 (2018).
48. W. L. Jorgensen, J. Chandrasekhar, J. D. Madura, R. W. Impey, M. L. Klein, Comparison of simple potential functions for simulating liquid water. *J. Chem. Phys.* **79**, 926–935 (1983).
49. J. Lee, X. Cheng, J. M. Swails, M. S. Yeom, P. K. Eastman, J. A. Lemkul, S. Wei, J. Buckner, J. C. Jeong, Y. Qi, S. Jo, V. S. Pande, D. A. Case, C. L. Brooks 3rd, A. D. MacKerell Jr, J. B. Klauda, W. Im, CHARMM-GUI Input Generator for NAMD, GROMACS, AMBER, OpenMM, and CHARMM/OpenMM Simulations Using the CHARMM36 Additive Force Field. *J. Chem. Theory Comput.* **12**, 405–413 (2016).
50. S. E. Feller, Y. Zhang, R. W. Pastor, B. R. Brooks, Constant pressure molecular dynamics simulation: The Langevin piston method. *J. Chem. Phys.* **103**, 4613–4621 (1995).
51. G. J. Martyna, D. J. Tobias, M. L. Klein, Constant pressure molecular dynamics algorithms. *J. Chem. Phys.* **101**, 4177–4189 (1994).
52. J.-P. Ryckaert, G. Ciccotti, H. J. C. Berendsen, Numerical integration of the cartesian equations of motion of a system with constraints: molecular dynamics of n-alkanes. *J. Comput. Phys.* **23**, 327–341 (1977).
53. T. Darden, D. York, L. Pedersen, Particle mesh Ewald: An N·log(N) method for Ewald sums in large systems. *J. Chem. Phys.* **98**, 10089–10092 (1993).
54. A. Harasima, "Molecular theory of surface tension" in *Advances in Chemical Physics* (John Wiley & Sons, Inc., Hoboken, NJ, USA, 2007), *Advances in chemical physics*, pp. 203–237.
55. J. Sonne, F. Y. Hansen, G. H. Peters, Methodological problems in pressure profile calculations for lipid bilayers. *J. Chem. Phys.* **122**, 124903 (2005).
56. C. E. ZoBell, C. H. Oppenheimer, Some effects of hydrostatic pressure on the multiplication and morphology of marine bacteria. *J. Bacteriol.* **60**, 771–781 (1950).
57. A. Kusters, W. Dowhan, B. de Kruijff, Negatively charged phospholipids restore prePhoE translocation across phosphatidylglycerol-depleted Escherichia coli inner membranes. *J. Biol. Chem.* **266**, 8659–8662 (1991).
58. Y. Asai, Y. Katayose, C. Hikita, A. Ohta, I. Shibuya, Suppression of the lethal effect of acidic-phospholipid deficiency by defective formation of the major outer membrane lipoprotein in Escherichia coli. *J. Bacteriol.* **171**, 6867–6869 (1989).
59. H. Hata, M. Nishiyama, A. Kitao, Molecular dynamics simulation of proteins under high pressure: Structure, function and thermodynamics. *Biochimica et Biophysica Acta (BBA) - General Subjects.* **1864**, 129395 (2020).
60. B. Wroblowski, J. F. Díaz, K. Heremans, Y. Engelborghs, Molecular mechanisms of pressure induced conformational changes in BPTI. *Proteins: Structure, Function, and Genetics.* **25**, 446–455 (1996).
61. D. B. Kitchen, L. H. Reed, R. M. Levy, Molecular dynamics simulation of solvated protein at high pressure. *Biochemistry.* **31**, 10083–10093 (1992).
62. G. Sgourakis, R. Day, S. A. McCallum, A. E. Garcia, Pressure Effects on the Ensemble Dynamics of Ubiquitin Inspected with Molecular Dynamics Simulations and Isotropic Reorientational Eigenmode Dynamics. *Biophys. J.* **95**, 3943–3955 (2008).

63. L. Meinhold, J. C. Smith, Pressure-dependent transition in protein dynamics at about 4 kbar revealed by molecular dynamics simulation. *Physical Review E*. **72**, 061908 (2005).
64. Wakai, K. Takemura, T. Morita, A. Kitao, Mechanism of Deep-Sea Fish α-Actin Pressure Tolerance Investigated by Molecular Dynamics Simulations. *PLoS One*. **9**, e85852 (2014).
65. M. Marchi, K. Akasaka, Simulation of Hydrated BPTI at High Pressure: Changes in Hydrogen Bonding and Its Relation with NMR Experiments. *J. Phys. Chem. B*. **105**, 711–714 (2001).
66. F. W. Starr, F. Sciortino, H. E. Stanley, Dynamics of simulated water under pressure. *Physical Review E*. **60**, 6757–6768 (1999).
67. K. Akasaka, H. Matsuki, Eds., *High Pressure Bioscience: Basic Concepts, Applications and Frontiers* (Springer Netherlands, Dordrecht, 2015), vol. 72 of *Subcellular Biochemistry*.
68. M. Kusube, H. Matsuki, S. Kaneshina, Thermotropic and barotropic phase transitions of N-methylated dipalmitoylphosphatidylethanolamine bilayers. *Biochimica et Biophysica Acta (BBA) - Biomembranes*. **1668**, 25–32 (2005).
69. H. Ichimori, T. Hata, H. Matsuki, S. Kaneshina, Barotropic phase transitions and pressure-induced interdigitation on bilayer membranes of phospholipids with varying acyl chain lengths. *Biochimica et Biophysica Acta (BBA) - Biomembranes*. **1414**, 165–174 (1998).
70. R. Sueyoshi, K. Tada, M. Goto, N. Tamai, H. Matsuki, S. Kaneshina, Barotropic phase transition between the lamellar liquid crystal phase and the inverted hexagonal phase of dioleoylphosphatidylethanolamine. *Colloids Surf. B Biointerfaces*. **50**, 85–88 (2006).
71. W. Helfrich, Elastic Properties of Lipid Bilayers: Theory and Possible Experiments. *Zeitschrift für Naturforschung C*. **28**, 693–703 (1973).
72. B. Canham, The minimum energy of bending as a possible explanation of the biconcave shape of the human red blood cell. *J. Theor. Biol*. **26**, 61–81 (1970).
73. A. Waugh, E. A. Evans, Thermoelasticity of red blood cell membrane. *Biophys. J*. **26**, 115–131 (1979).
74. M. Kaltenegger, J. Kremser, M. P. K. Frewein, P. Ziherl, D. J. Bonthuis, G. Pabst, Intrinsic lipid curvatures of mammalian plasma membrane outer leaflet lipids and ceramides. *Biochimica et Biophysica Acta (BBA) – Biomembranes*. **1863**, 183709 (2021).
75. P. Khakbaz, J. B. Klauda, Investigation of phase transitions of saturated phosphocholine lipid bilayers via molecular dynamics simulations. *Biochimica et Biophysica Acta (BBA) - Biomembranes*. **1860**, 1489–1501 (2018).
76. K. Uppulury, P. S. Coppock, J. T. Kindt, Molecular Simulation of the DPPE Lipid Bilayer Gel Phase: Coupling between Molecular Packing Order and Tail Tilt Angle. *J. Phys. Chem. B*. **119**, 8725–8733 (2015).
77. K. Tu, D. J. Tobias, J. K. Blasie, M. L. Klein, Molecular dynamics investigation of the structure of a fully hydrated gel-phase dipalmitoylphosphatidylcholine bilayer. *Biophys. J*. **70**, 595–608 (1996).
78. M. Venable, B. R. Brooks, R. W. Pastor, Molecular dynamics simulations of gel (LβI) phase lipid bilayers in constant pressure and constant surface area ensembles. *J. Chem. Phys*. **112**, 4822–4832 (2000).
79. E. Evans, W. Rawicz, Elasticity of "Fuzzy" Biomembranes. *Phys. Rev. Lett*. **79**, 2379–2382 (1997).
80. E. Fahy, S. Subramaniam, R. C. Murphy, M. Nishijima, C. R. H. Raetz, T. Shimizu, F.

Spener, G. van Meer, M. J. O. Wakelam, E. A. Dennis, Update of the LIPID MAPS comprehensive classification system for lipids. *J. Lipid Res.* **50**, S9–S14 (2009).

Acknowledgements: Sol Gruner, George Somero, and Douglas Bartlett contributed discussion that informed the direction of this work. Caitlyn Webster, Charlotte Havermans, Stefanie Meyer, Lynne Christianson, Shannon Johnson, and Darrin Schultz collected ctenophores for this study. Crews of the *R/V Western Flyer*, *R/V Rachel Carson*, *R/V Ka'imikai-O-Kanaloa*, *R/V Kilo Moana*, ROV Doc Ricketts, and ROV Ventana provided field support. Qingqiu Huang provided HPSAXS technical support.

Funding:

National Aeronautics and Space Administration postdoctoral fellowship 0017-NPP-MAR22-A-Astrobio (JRW)

National Institutes of Health grant 5T32EB009380-14 (DM)

National Institutes of Health grant GM139641 (EAD)

National Science Foundation grants MCB-2121854, MCB-2316457 (EL)

National Science Foundation grants DEB-1542679, OCE-1829805, MCB-2316456 (SHDH)

National Science Foundation grants MCB-2046303, MCB-2316458, IOS-2040022 (IB)

Office of Naval Research grant N00014-23-1-2543 (IB)

CHEXS is supported by National Science Foundation award DMR-1829070 and the MacCHESS resource is supported by National Institutes of Health award 1-P30-GM124166-01A1 and the New York State Foundation for Science, Technology and Innovation.

Author Contributions:

Conceptualization: JRW, SHDH, IB

Methodology: JRW, AMA, OQ, AS, REG, EL, IB

Investigation: JRW, DM, SJV, MAP, AMA, OQ, AS, REG, EL, SHDH, IB

Visualization: JRW, DM, EL, SHDH

Funding acquisition: REG, EAD, EL, SHDH, IB

Project administration: SHDH, IB

Supervision: EAD, EL, SHDH, IB

Writing – original draft: JRW, IB

Writing – review & editing: JRW, DM, SJV, OQ, AS, REG, EAD, EL, SHDH, IB

Competing interests: Authors declare that they have no competing interests.

Data and materials availability: Raw data, analysis, and visualization code are available at https://github.com/octopode/deeplipid-biophys-2023.

Supplementary Materials

Materials and Methods

Supplementary Text

Figs. S1 to S10

Tables S1 to S3

References (*30-80*)

Movie S1

Data S1

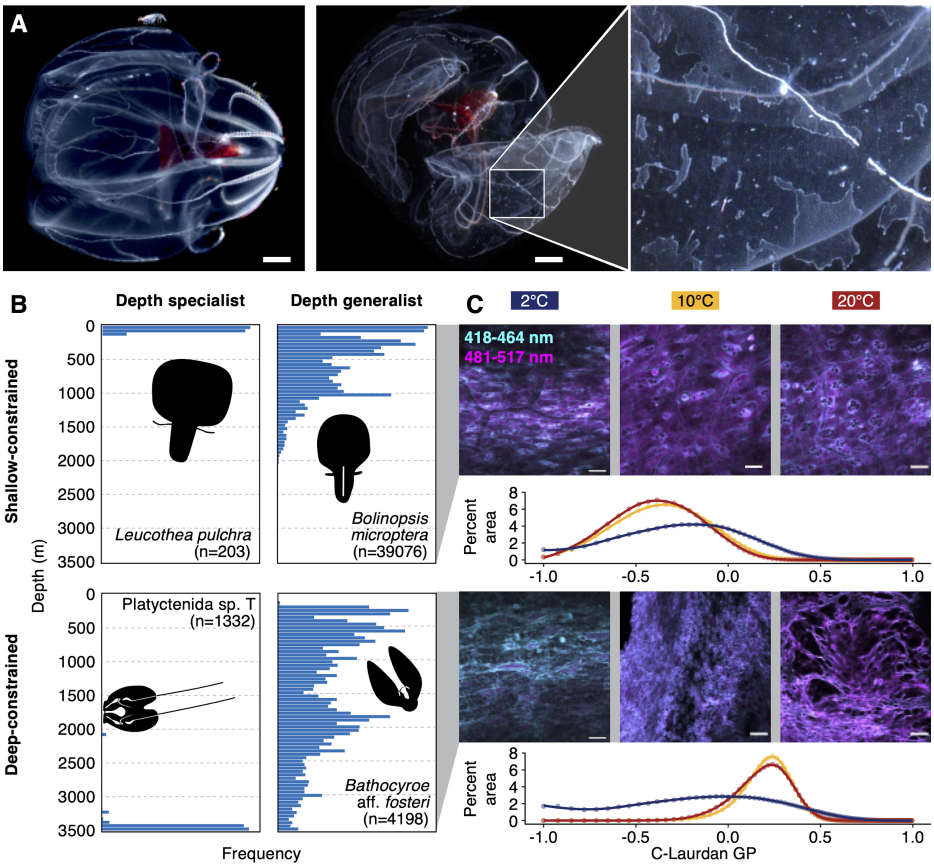

Fig. 1. Ecological and physiological evidence for pressure specialization in ctenophores. (**A**) Disintegration of the deep-constrained ctenophore *Bathocyroe* aff. *fosteri* at atmospheric pressure. The left image was taken in the specimen's native water at 2°C, immediately after recovery from the ROV. The right image is of the same animal and was taken 10 minutes later at 4°C. Scale bars, 5 mm. Inset shows disintegration of the ectodermal tissue. (**B**) Depth distributions of four ctenophore species with narrow, broad, shallow, and deep depth ranges. (**C**) Live *ex vivo* tissue mounts stained with solvatochromic C-Laurdan membrane label and imaged at increasing temperatures. Images are a composite of two emission ranges, which are used to calculate GP ratios. In *Bolinopsis microptera*, which occurs from 0-2000 m, GP value decreases with increasing temperature indicating a more fluid lamellar phase. In *Bathocyroe*, which occurs down to >3500 m but not shallower than 200 m, GP displays a sharp increase between 2 and 10°C, concurrent with a catastrophic collapse of membrane morphology. This increase in GP patterns is observed in synthetic lipid systems undergoing inversion (Figs. S3C, S8D). Scale bars, 10 µm.

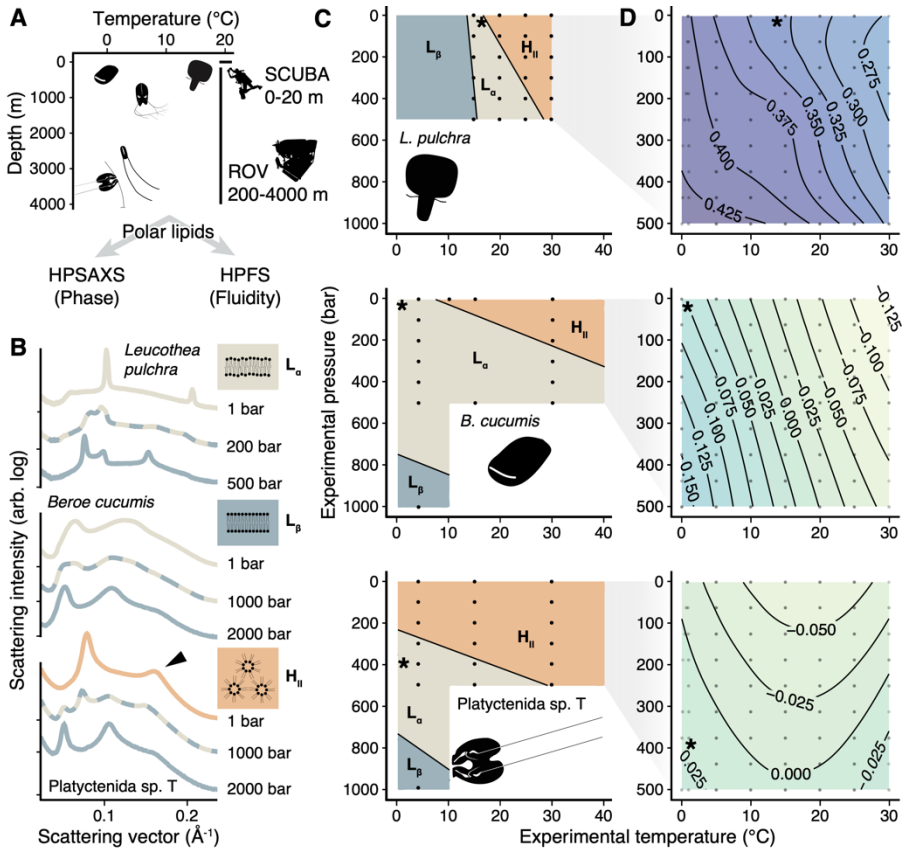

Fig. 2. Biophysical signatures of depth-adaptation. (**A**) Schematic of the pipeline carried out on a set of ctenophores collected in different P-T regimes. Polar lipids were isolated from collected animals and analyzed by HPSAXS for phase properties and HPFS for membrane fluidity. (**B**) Representative SAXS profiles used to determine the phase of total polar lipid dispersions from the shallow Arctic ctenophore *Beroe cucumis* (profiles shown at 4°C), the deep-constrained Platyctenida sp. T (4°C), and the shallow-constrained *Leucothea pulchra* (15°C). Profiles are colored by phase composition and baselines are offset for clarity. The broad peak indicated in Platyctenida sp. T results from the overlap of two close peaks characteristic of the H_{II} phase. The three main phases are shown in the inset cartoons. (**C**) Phase change diagrams for the same dispersions based on SAXS data. Points mark measured states and asterisks indicate the native P-T for each animal. (**D**) C-Laurdan GP values for liposomes from the same samples measured across a P-T grid. Within lamellar phase regions, GP reflects lipid ordering, with lower values corresponding to more fluid membranes. Near native conditions, GP pressure-sensitivity was greater in shallow than in deep samples. This sensitivity is reflected by the proximity of contour lines.

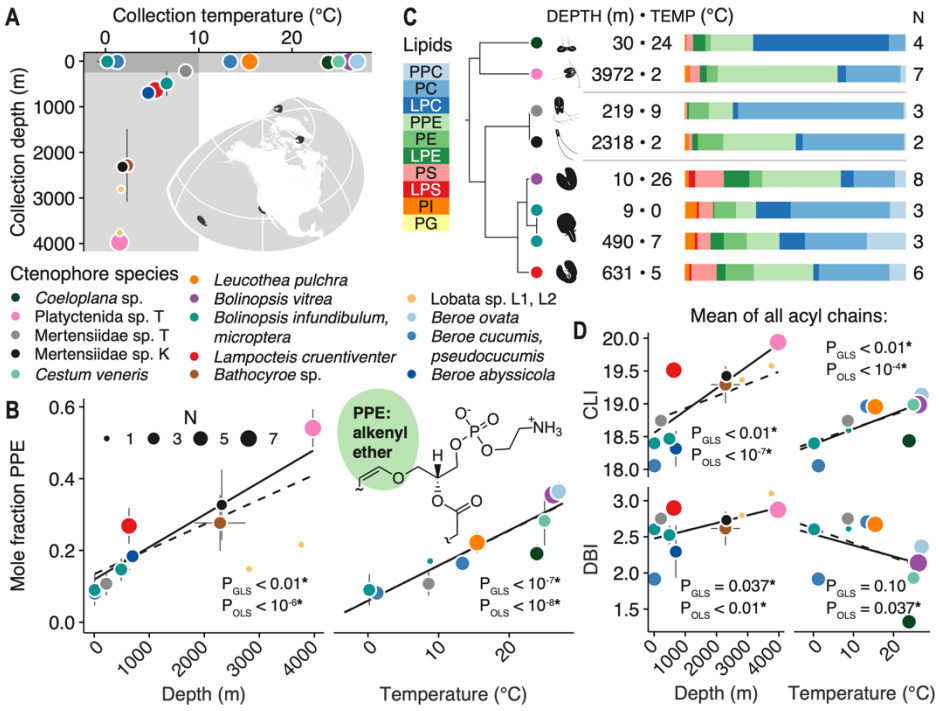

Fig. 3. Lipidomic analysis of ctenophore phospholipids. (**A**) Plot showing the depth and temperature regimes of the 66 ctenophores in the dataset. Each data point represents the mean for one of the 17 species collected; all error bars are +/- SEM. Subsets of the collections made ≤10°C and ≤250 m depth, shaded in gray, were used to assess depth and temperature trends, respectively. Collection locales are marked on the globe in black. (**B**) High relative abundance of PPE is correlated with both deep-cold and shallow-warm habitats. Structure of the PPE alkenyl ether linkage is inset. Ordinary least-squares regressions (OLS, solid lines) and phylogenetically generalized ones (GLS, dashed lines) are shown with their corresponding P-values; an asterisk indicates significance at the $\alpha \leq 0.05$ level (Welch's *t* test). (**C**) Examples of independent lipidomic depth-adaptation in three ctenophore clades, delimited with gray lines. Phylogenetics have revealed that ctenophores have depth-specialized on multiple occasions. Within each clade, deeper cold species have higher fractions of PPE and PE, and lower fractions of PC and lysolipids. Temperature specialization of a shallow, tropical representative of genus *Bolinopsis* is also shown. (**D**) Phospholipid total chain length index (CLI) and unsaturation (double bond index; DBI) as a function of depth and temperature. Deeper cold lipidomes feature longer and more unsaturated acyl chains, while colder shallow lipidomes feature shorter and more unsaturated acyl chains. Regressions are shown as in **B**.

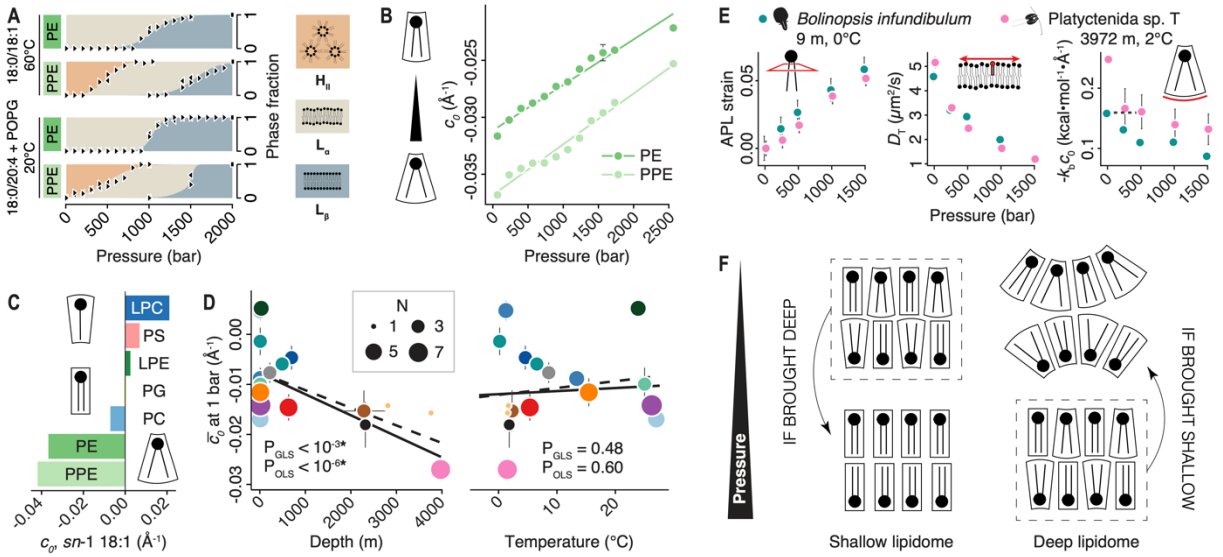

Fig. 4: Exploring the role of lipid curvature in deep-sea lipidomes enriched in PPE. (**A**) Lipid phase ratios estimated from HPSAXS data plotted as a function of pressure and of the PPE headgroup. At the temperatures tested, PPE was H_{II}-phase and PE was L_{α}-phase at 1 bar regardless of whether the *sn*-2 acyl chain was poly- or monounsaturated. The polyunsaturated phospholipids were chosen as the closest commercially available analogues to those in ctenopohres; 5 mole percent PG was added to bring the inverted phase transition within an instrumentally achievable P-T domain. Each black triangle denotes an individual X-ray exposure taken during a pressure sweep in the indicated direction. Black squares at upper right are exposures taken at maximum pressure. (**B**) Spontaneous curvature (c_0) values measured for PPE and PE species with a monounsaturated *sn*-2 chain. Cartoons by the vertical axis illustrate the relationship between c_0 and lipid shape. PPE shows a stronger negative curvature than PE and the effect of pressure on both is identical. Neutral-plane c_0 was inferred by fitting global models to HPSAXS profiles of the lipids (20%) hosted in a di-oleoyl PE (DOPE) H_{II} phase and relaxed with 10.7% w/w 9(Z)-tricosene. (**C**) Representative c_0 values for phospholipid classes. These were used along with linear corrections for *sn*-1 acyl chain structure (Materials and Methods) to estimate the mean phospholipid curvature at 1 bar ($\overline{c_0}$) for all measured lipidomes. (**D**) The robust correlation of $\overline{c_0}$ with habitat depth among all animals sampled; deeper lipidomes feature a higher degree of lipidome curvature. Habitat temperature does not predict $\overline{c_0}$. Regressions are shown as in Fig. 3. (**E**) Comparison of simulated lipidomes modeled after a cold, shallow species (*B. infundibulum*) and a deep species (Platyctenida sp. T) Pressure-dependent properties include area per lipid (APL) strain relative to 1 bar, average lipid translational diffusion rate (D_T), and the first moment of the computed lateral stress profile, which is equal to $-k_b c_0$. All simulations were run at 20°C. For $-k_b c_0$, the pressure equivalency of shallow and deep systems is indicated with a dashed line. Simulation snapshots and additional details are shown in Fig. S7. (**F**) A homeocurvature adaptation model in which a more negative baseline (1 bar) lipidome curvature is required to offset the effects of high pressure on lipid shape. For lipidomes of both shallow- and deep-living species, physiological membrane states (dashed boxes) contain a mixture of bilayer and non-bilayer lipids, but the chemistry of these species must differ to maintain this arrangement. When membranes from shallow-living animals were compressed, lipidome curvature was lost, potentially disrupting membrane dynamics and plasticity. When membranes

from deep-living animals were decompressed, negative lipidome curvature increased, destabilizing membrane structure.

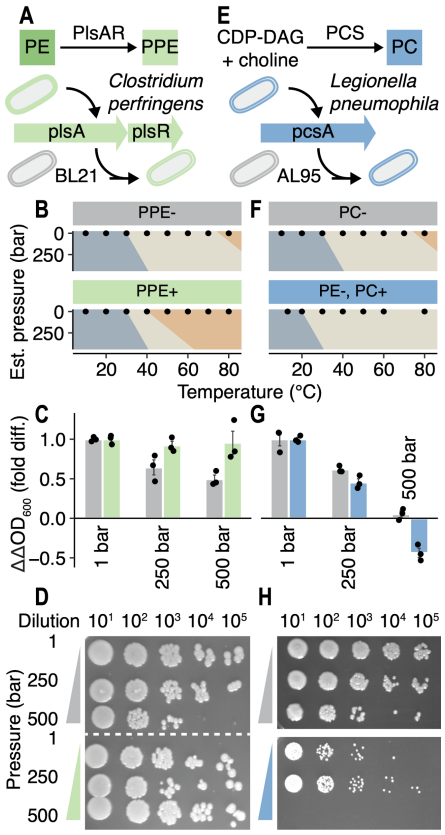

Fig. 5. Testing the principles of pressure adaptation in engineered bacterial cells. (**A**) Heterologous synthesis of PPE, using plasmid-based expression of the plsAR PE reductase from *Clostridium*, enhances *E. coli* lipidome curvature and its propensity to invert into H_{II}, as assayed by SAXS as a function of temperature. (**B**) Phase diagrams of *E. coli* polar lipids (inner and outer membrane) in PPE- (BL21 + pET28a, gray) and PPE+ (BL21 + pPlScp, green) strains. To facilitate comparison with the pressure treatments, these diagrams are extrapolated along a pressure axis using published temperature-pressure equivalencies (*24*). (**C**) Growth of PPE-lacking and PPE-containing *E. coli* in microaerobic culture under pressure. The difference in pressure-sensitivity of growth was significant ($P = 0.009$, multiple regression with F-test). (**D**) Post-decompression survival was similarly rendered pressure-insensitive by PPE (compare lower right colonies in both panels.) (**E**) Non-native synthesis of PC, using plasmid-based expression of the PC synthase (PCS) from *Legionella* in the PE-free background AL95, reduces lipidome curvature and propensity to invert into H_{II}. (**F**) Pressure-extrapolated phase diagrams of *E. coli* polar lipids in PC- (AAL9256 with an integrated P_{BAD}-pssA cassette, gray) and PE-, PC+ (AL95 + pPCSlp, blue) strains. (**G**) Growth and (**H**) survival were assessed as in **C** and **D**, except that outgrowth prior to pressurization was aerobic. The difference in pressure-sensitivity of growth was significant ($p = 0.002$), and the PC strain was inviable at 500 bar. Strain pairs were chosen to minimize differences in genetic background and promoters were identical within each pair.